The Effect of Impurities on the Evolution of the Melting Front, Analyzed in a Two-Dimensional Representation for the Eutectic Pt-C

P. Castro,[1, 3] P. Bloembergen,[2] W. Dong[2]

[1] University of Cantabria, Santander, 39005, Spain

[2] National Institute of Metrology, NIM, Beijing, 100013, China

[3] To whom correspondence should be addressed. E-mail: castropb@unican.es

Abstract

The paper discusses the effect of two-front melting on the liquidus temperature of the eutectic Pt-C and the eutectic temperature of the system in its pure state. This influence factor has not been considered thus far in the uncertainty budget associated with the assignment of thermodynamic temperatures to the eutectics Co-C (1597.15 K), Pt-C (2011.05 K), and Re-C (2747.35 K), selected in the European Metrology Research Programme project Implementing the New Kelvin. For Pt-C, simulation of the effect of two-front melting on the melting process has been done before in a 1D analytical model, and this formed the starting point to the present study. In this study the melting process is analyzed by means of a 2D axisymmetrical finite volume model. In the model, freezing and melting are considered for an impure ingot and for a pure ingot. As to the impure ingot, the impurity concentrations are the concentrations met in current practice of the realization of the high-temperature reference fixed point, but formulated in terms of an effective concentration and associated effective distribution coefficient $k < 1$, related to a Scheil fit to the melting curve at given melting conditions as measured for the eutectic Pt-C. Heat injection rates for melting are varied from 15 000 $W \cdot m^{-2}$ down to 3000 $W \cdot m^{-2}$. In any case for the impure system, two melting fronts are showing up. For the pure system, only one melting front is generated, traveling from the outside of the ingot towards its inside.

Keywords: High-temperature fixed point; Impurity distribution; Melting front

1 Introduction

This study forms part of the European Metrology Research Programme project Implementing the New Kelvin to assign thermodynamic temperatures to a selected set of high-temperature fixed points (HTFPs), namely, the eutectics Co-C (1597.15 K), Pt-C (2011.05 K), and Re-C (2747.35 K) [1, 2]. Here, by way of example, we concentrate on the system Pt-C. The standard uncertainty $u(T_E)$ in the eutectic temperature T_E, associated with the system in its pure state, obtained when following standard procedures, has been estimated by Bloembergen in "Operational Characteristics of High-Temperature Reference Points. Data Analysis and Uncertainty Budget" as 0.06 K. However, the uncertainty analysis did not consider the feature of two-front melting, the main topic of this paper. The transition temperature of the pure system T_E, has to be referred to, when qualifying high-temperature reference points, utilized to underpin a temperature scale, such as to get a univocal reference temperature. Note that the estimate of 0.06 K refers to the uncertainty associated with the realization of the fixed point (Pt-C) in question, including the correction for the effect of impurities, but it does not include the uncertainty in the measurement of the absolute radiance temperature around T_E.

The present study is an extension of a previous one-dimensional study [3] to two dimensions. The previous study derived the profile T_m, in terms of the liquid-solid interface temperature across the ingot of the eutectic Pt-C, embedded during the preceding freeze, from the melting curve $T_{cav}(t)$ as observed by a radiation thermometer viewing the cavity bottom of the cell in which it is contained. T_m is associated with an impurity spectrum, where impurities with distribution coefficients $k < 1$ are predominant [4] which is a feature common to M-C eutectics selected as ingot materials for high-temperature fixed points, and segregated over the ingot during the preceding freeze. The derivation referred to was based upon an iterative procedure.

In the one-dimensional analysis, the actual cup-shaped ingot was simulated by a square slab with an equivalent volume of the ingot. The cavity bottom was simulated by the graphite slab to the left side of the ingot, its thickness being set to that of the actual cavity bottom. The analysis was tightly related to results obtained for the cell Pt-C #5 studied in [5], a cell of hybrid construction, with the ingot being surrounded by a graphite sleeve separated from the crucible by two layers of grafoil.

In this new study, the actual Pt-C #5 cell was modeled considering heat transfer in two dimensions with several boundary conditions set at the cell walls. The methodology was varying the cell heat injection rate Q at a given heat extraction rate Q_f = -3000 W·m^{-2} of the preceding freeze, corresponding with a temperature offset (T - T_f) = −5 K, T_f referring to the freezing temperature. For the given rate of the freeze, the evolution of the liquid-solid interface in the course of the subsequent melting process for different melting rates was studied. A pure and an impure system were modeled and compared. For the pure system only, one melting front is generated, traveling from the outside of the ingot towards its inside. In the impure

system, described by an effective Scheil function, in any case two-front melting was induced, the evolution of the fronts with time depending on the impurity level and the heat injection rates.

2 Two-Dimensional Model

The cell was represented by an axisymmetrical model [6, 7] with heat injection and extraction rates as boundary conditions. As shown in Fig. 1, the influence of the furnace was simulated by heat losses from the aperture of the cavity and the front wall of the cell. The furnace itself was not considered in the model so as to decrease computing time and to keep the system as simple as possible in order to just focus on the study of the evolution of the liquid/solid interface(s) under varying melting conditions, as shown in Fig. 1.

In the model, freezing and melting were considered for an impure ingot and for a pure ingot. T_m, referred to above, representing the evolution of the liquid-solid interface temperature across the impure ingot during the freeze preceding any of the melts, considered below, is described by an effective Scheil function:

$$T_m(t) - T_E = mcF(t)^{k-1} \tag{1}$$

where F is the liquid fraction, T_E is the eutectic temperature of the pure system, c is the impurity concentration, m *is* the associated liquidus slope, and k is the distribution coefficient. The ternary eutectic point (T_{eut}, c_{eut}) was introduced in the model by the definition,

$$c_{eut} = (T_{eut} - T_E)m^{-1} \tag{2}$$

In Eq. 2 T_{eut} is the minimum melting temperature at the ternary eutectic concentration c_{eut}, which assumes that the liquidus and solidus are linear between $c = 0$ and $c = c_{eut}$ and $c = kc_{eut}$, respectively [8]. With these parameters, the liquidus and solidus can be expressed in relation to c, as follows:

$$T_{liq}(c) = T_E + mc \tag{3}$$

$$T_{sol}(c) = T_E + mck^{-1} \tag{4}$$

That actually the solidification comes to completion at a finite solidus temperature T_{sol} = 2008.43 K, (given by the maximum in slope of the measured curve, just prior to the melting plateau) in contrast to what the Scheil expression predicts for impurities with distribution coefficients $k < 1$, has to do with the increase of the impurity concentrations in the liquid phase to very high levels in the course of the Scheil freezing process. This implies that eventually the system surpasses phase boundaries or is trapped in singular points, such as a ternary eutectic point $T_{eut} = T_{sol}$ in the ternary phase space, as assumed above. The parameter values associated with T_m are given in Table 1.

The liquid fraction F, calculated by the model, indicates the fraction of the cell volume that is in a liquid form associated with each cell in the domain and it is computed based on an enthalpy balance. The region in which the liquid fraction lies between 0 and 1 is called the mushy zone and it is modeled as a pseudo-porous medium in which the porosity decreases from 1 to 0 as the material solidifies.

T_{backwall} represents the observed temperature of the back wall of the cavity, and is here obtained as an output of the model, and derived from the input parameter T_{m}. It will be compared with T_{cav}, the actually observed temperature, represented also by a Scheil function extrapolated to the liquidus point with the parameters shown in Table 2, together with those derived for T_{backwall}. This reverse procedure is adopted here to avoid the cumbersome process of iteration in combination with finite-volume analysis when aiming at deriving T_{m} from T_{cav}, as in the 1D case, where just an analytical approach was combined with iteration. Note that in these definitions F is an output of the numerical model.

The melting experiment serving as the experimental basis to this study was induced by a 20 K furnace-temperature offset, $T_{\text{furnace}} - T_{\text{E}}$, with respect to the eutectic temperature, at a 20 K·min^{-1} ramping rate, preceded by a freeze at an offset of −5 K. In this application offsets used in the experiment were converted to heat extraction and heat injection rates for freezing and melting, respectively. The heat extraction rate for freezing was taken as $Q_{\text{f}} = -3000$ W·m^{-2}, corresponding with an offset of -5 K. Heat injection rates, Q, for melting varied from 15 000 W·m^{-2} to 10 000 W·m^{-2} to 5000 W·m^{-2}, and 3000 W·m^{-2}, corresponding with offsets of +25 K, +16.7 K, +8.3 K, and +5 K, respectively. The determinants to this process were the heat injection rate, thermal conductivity of the ingot, the overall impurity concentration, and the distribution coefficient k associated with the impurity in question. The ratio between the thermal conductivities of the liquid and solid phases was taken as 0.5. Thermophysical properties of the materials involved are shown in Table 3.

3 Results and Discussion

The results are presented in two ways:

(a) As output parameters, given as a function of time, t, and position, x, over the cross section indicated in Fig. 1 behind the back wall of the crucible describing (a) the evolution of the impurity concentration $_C(x,t)$ during the preceding freeze, $Q_{\text{f}} = -3000$ W·m^{-2}, Figs. 2 and 3, and (b) the evolution of the melting front in terms of $F(t)$, $Q = 3000$ W·m^{-2}, Fig. 4.

(b) As output parameters, averaged over the total of the alloy material, describing (a) $T_{\text{backwall}}(F)$, $T_{\text{cav}}(F)$, and $T_{\text{m}}(F)$ for $Q = 3000$ W·m^{-2} and $Q = 15\ 000$ W·m^{-2}, Fig. 5, where the F values have been obtained by the numerical model and (b) $T_{\text{backwall}}(t)$ and $T_{\text{backwall}}(F)$ as a function of Q, Figs. 6 and 7.

3.1 Results Obtained for $c(x, t)$ and $F(x,t)$

The evolution of the freezing and melting front was studied along a perpendicular line to the back wall of the cell with the x coordinate in the axis direction as shown in Fig. 1.

During freezing (from t = 0 s to t = 2800 s) from the outside with Q_f = -3000 W·m^{-2}, the evolution of the impurity concentration $c(x, t)$ towards the inside wall of the cell is shown in Fig. 2. The impurity distribution when the freeze ended (t = 2800 s), additionally illustrated in Fig. 3, is the one with which the melt starts. Since for Scheil freezing, impurities with a distribution coefficient $k < 1$ are rejected into the liquid, the impurity concentration will pile up towards the inside of the ingot during freezing, starting from its outside, as demonstrated in Fig. 2, where the inside of the ingot is located at the right side of the figure. Therefore, an inside melting front will appear during melting, following outside freezing at a moderate freezing rate Q_f = -3000 W·m^{-2}. This inhomogeneous impurity distribution was studied for different Q_f's showing an increase of the impurity concentration near the inside crucible wall as the freeze was slower (lower Q_f).

In addition, because of the lack of available data for the mass diffusivity at this high temperature, a parametric study was carried out for different mass diffusivity values of impurities in the liquid phase giving a higher average impurity concentration in the liquid phase during freezing as the mass diffusivity increased and no significant inhomogeneous impurity distribution, approaching the concentration c in the fully liquid state, for values of mass diffusivity lower than 10^{-6} m^2·s^{-1}.

The value for $F(x, t)$ during melting was plotted versus the x coordinate in Fig. 4 to show the creation of the two fronts for Q = 3000 W·m^{-2}. In all the cases considered, eventually two melting fronts are showing up, associated with the two local maxima in the curves, shown in Fig. 4. In this figure the mushiness of (parts of) the structure between the start of melting (t = 3400 s), where the sample is still in the fully solid state (F = 0) and the end of melting (t = 5400 s), where the sample is just in its fully liquid state (F = 1) is clearly showing up.

As shown in Fig. 8d to f, discussed more fully below, for the highest rate Q = 15 000 W·m^{-2}, outside melting is prominent, inside melting starting at the end of the melting process. For the lower rates, inside melting is enhanced, the melting front being completed and in full development before the outside front has been established. See Fig. 8a to c for Q = 3000 W·m^{-2}. Whereas for Q = 5000 W·m^{-2}, the inside front is still developing during melting; for Q = 15 000 W·m^{-2}, the inside front is coming to a stand-still just after its completion. It might well be that at still higher melting rates, melting will develop from the outside of the ingot only. This is because of the preceding freeze ending at a finite solidus point, $T_{sol} = T_{eut}$, implying that the slope of the freezing profile in terms of the liquid-solid interface versus time remains finite at the end of freezing. At a heat injection rate associated with a slope of the temperature gradient over the liquid phase, larger than the finite slope of the freezing profile at the inside of the ingot, melting would proceed from the outside only. This aspect was not considered in the 1D model [3].

3.2 $T_{backwall}(F)$, $T_{cav}(F)$, and $T_m(F)$

Figure 5 shows (a) $T_{backwall}$, as simulated for the impure system for Q = 3000 W·m^{-2} and Q = 15 000 W·m^{-2}, (b) the liquid-solid interface temperature T_m, Q_f = -3000 W·m^{-2} established during the preceding freeze (derived in the 1D model), and (c) the actually measured temperature T_{cav} for Q = 12 000 W·m^{-2} (in Scheil representation). T_m served as a reference to T_{cav} (in the 1D study) and is likewise to serve as a reference to $T_{backwall}$ (in the underlying 2D simulation). For F = 0.5 it is found that T_m - $T_{backwall}$ = 38 mK and 87 mK for Q = 3000 W·m^{-2} and Q = 15 000 W·m^{-2}, respectively, and T_m - T_{cav} = 129 mK. This shows that the relation between the experimental curve T_{cav} (in Scheil representation) and T_m is different from that between $T_{backwall}$ (the "measured curve," as predicted in 2D simulation) and T_m, where T_m is the characteristic of the preceding freeze in both the 1D and 2D cases, the difference depending on the heat injection rate associated with $T_{backwall}$.

However, the smaller temperature difference, T_m - $T_{backwall}$, in 2D, as compared with T_m - T_{cav} in 1D, shown in Fig. 5, is in part due to the fact that radiative interactions between the cavity cylindrical section and the back wall of the cavity in 2D/3D, absent in 1D, lead to a reduction of the temperature drop across the cavity bottom in 2D. But it is mainly due to the higher heat injection rate (of Q = 12 000 W·m^{-2}, at a temperature offset of +20 K), associated with the experimental melting curve T_{cav}, leading to a downward shift of T_{cav} with respect to $T_{backwall}$, the latter being obtained at Q = 3000 W·m^{-2}. For $T_{backwall}$, Q = 15 000 W·m^{-2}, there is reasonable consistency between the results obtained in 1D and 2D.

3.3 $T_{backwall}(t)$ as a Function of Q

In Fig. 6 the melting plateaus are shown for different heat injection rates, together with the curve of the preceding freeze (Q_f = -3000 W·m^{-2}). The step near the end of the melting curve is associated with thermal bridging being initiated, near the back wall of the cavity [9]. This is corroborated by the plots shown in Fig. 7. From an inspection of Fig. 6, it seems that, overall, the melting temperature, as observed, is lower than the freezing temperature. This is probably in part due to the circumstance that because of thermal bridging near the end of the melting process, in fact, the melting curves are cut off from reaching the actual liquidus temperature, and thus the curves are, as it seems, shifted downward with respect to the freezing curve, for which at the liquidus temperature thermal bridging is not interfering at all.

In Fig. 7 the melting plateaus for different heat injection rates as a function of the liquid fraction F are represented. Thermal bridging is showing up as the steep upturn, following the melting plateau. The higher the melting rate, the closer is the upturn to F = 1, as further discussed below. A slight decrease of the point of inflection temperature, associated with the upturn, is also observed for faster melts.

At a low heat injection rate, say Q = 3000 W·m^{-2}, thermal bridging occurs at a relatively low liquid fraction, where the well-developed inside and outside fronts meet about midway the stretch between the

outside and inside of the ingot, away from the rim of the cavity cone. In contrast, at a high injection rate, say Q = 15 000 W·m^{-2}, thermal bridging occurs at a relatively high liquid fraction, where the outside front meets the quite restricted inside front close to the inside of the ingot, and near the rim of the cavity cone. All in all, the shift in thermal bridging towards $F = 1$ is correlated with the inside melting front shrinking with an increase in the heat injection rate, with the outside melting getting the upper hand. This is further corroborated by the snapshots shown in Fig. 8 for Q = 3000 W·m^{-2} and Q = 15 000 W·m^{-2} impure systems and Q = 3000 W·m^{-2} pure system. For these cases a snapshot is shown at the time where the inside melting front is just completed (Fig. 8a, d, and g), where thermal bridging is taking place (Fig. 8b, e, and h), and near the end of the melt where the region all around the cavity bottom, and a bit further, is surrounded by the liquid phase (Fig. 8c, f, and i).

Apparently, the higher the melting rate, the closer is the L/S interface to the cavity wall just before the occurrence of thermal bridging where the impurity concentration is highest. This may explain the observed decrease of the inflection point of the melting curve with increasing melting rate in Fig. 7. In addition, this provides a subsidiary explanation to the melting curves being shifted downwards with respect to the freezing curve in Fig. 6: the liquidus point of the freezing curve is associated with the lowest impurity concentration $c = 9.4\times10^{-5}$ mole fraction at the start of freezing.

From Fig. 8b and e where thermal bridging is taking place for Q = 3000 W·m^{-2} and Q = 15 000 W·m^{-2}, respectively, it might appear at first sight that the steep upturns, say in Fig. 6, marking the event of thermal bridging are situated at an unexpected large value of $F = F_{\text{infl}}$. But note that the sections not colored red in Fig. 8, also the blue parts, are in a mushy condition $0 < F < 1$, thus partly liquid, which explains the seemingly relative large values of F_{infl} in Fig. 6.

3.4 Error $\Delta(T_{\text{E}})$ in T_{E} When Disregarding the Effect of Two-Front Melting

Here we concentrate on the curves representing $T_{\text{backwall}}(F)$ for heat injection rates, Q = 3000 W·m^{-2} and Q = 15 000 W·m^{-2}, the extremes of the melting rates considered, in Fig. 5.

As demonstrated above for both injection rates, we would have two-front melting. For the ideal case of inside melting only, disregarding the effect of the furnace temperature gradient, we would have thermal bridging between the outside and inside of the ingot when, at the end of the melting process, the melting front reaches the outside of the cavity wall, i.e., at liquid fraction $F = F_{\text{liq}} = 1$, resulting in an abrupt upturn of the melting curve.

On the contrary for the real case of two-front melting, in question, the fronts will meet at some intermediate position between the inside and outside of the ingot, at intermediate liquid fraction $F_{\text{infl}} < 1$, and at an intermediate impurity concentration, $cF_{\text{infl}}{}^{k-1} > c$, at which event we will have thermal bridging between the outside and inside of the ingot, resulting in an abrupt upturn of the melting curve $T_{\text{backwall}}(t)$, as observed in the simulations.

Note that in practice such abrupt upturns, induced by two-front melting, may be blurred out by thermal bridging running in parallel, and induced by a furnace-temperature gradient, imposed upon the ingot, which is a more continuous process [10,11,12]. On the one hand, the latter effect is disregarded in our simulations, to just concentrate on the effect of two-front melting, but on the other hand, since the inflection point usually observed in the melting curve, as measured, is generally attributed to the furnace-temperature gradient effect, by this the effect of two-front melting is disregarded. By assuming that just inside melting is involved rather than two-front melting, as is the case, an error $\Delta T_E = mc(1 - F_{infl}^{k-1})$ in the eutectic temperature of the pure system would be made. For the curves Q = 3000 W·m^{-2} and Q = 15 000 W·m^{-2}, we have F_{infl} = 0.85 and F_{infl} = 0.94, respectively. For the error ΔT_E, with mc = −0.086 K, k = 0.316, Table 1, we get the results summarized in Table 4.

Still these results are well within the standard uncertainty $u(T_E)$ = 0.06 K attributed earlier to the eutectic Pt-C, disregarding the effect of two-front melting. This is due to the relatively low overall impurity concentration, in this case $c = 9.4\times10^{-5}$ mole fraction, characterizing ingots, chosen to represent eutectic reference fixed points.

This is always assuming that the melting curve $T_{backwall}(t)$, as observed, has been corrected for the temperature drop $\Delta T = \Delta T_b + \Delta T_L(t)$, across the cavity bottom, ΔT_b, and across the liquid phase between (inside) melting front and the back wall of the cavity wall, $\Delta T_L(t)$, such as to virtually coincide with the profile T_m up to F_{infl}. For Q = 3000 W·m^{-2} and Q = 15 000 W·m^{-2}, these corrections amount to about +0.03 K and +0.06 K, respectively, at $F = F_{infl}$, where thermal bridging is initiated, which thus cannot be neglected.

3.5 Pure System Compared with the Impure System

Finally, the comparison between a pure and an impure system for Q_f = -3000 W·m^{-2} and Q = 3000 W·m^{-2} is shown in Fig. 9, representing $T_{backwall}$ as a function of the liquid fraction F. For the pure system we have outside melting only. For the impure system it can be seen again how inside melting and thermal bridging made the measured temperature, as simulated, to sharply step up before completion of the melt. See also Fig. 7 and the snapshots in Fig. 8. For the pure case thermal bridging is a more continuous process distributed over a relatively deep melting front as also clarified in the associated snapshots in Fig. 8.

4 Conclusions

The effect of the impurity distribution on fixed-point temperature during freezing has been modeled, and its effect on the subsequent melt has been analyzed.

For all the melting heat injection rates, Q, from 15 000 W·m^{-2} to 3000 W·m^{-2} for the impure system considered, sharp upturns in the melting curve appeared, in agreement with what is often observed in the

experiments. The upturn is related to thermal bridging being initiated around the back wall of the cavity. It turned out that the lower the melting rate, the more pronounced is the inside melting front, whereas at higher melting rates, outside melting gets the upper hand. Only outside melting occurs for the pure system.

In the case of an impure system, in the earlier study in a one-dimensional representation, melting started always at the inside of the ingot and whether or not outside melting was induced, in addition, depended on the magnitude of the heat injection rate. On the other hand, in the two-dimensional representation studied here, it was found that always two melting fronts were involved within the range of heat injection rates considered. Whether or not we would have inside melting only for $Q < 3000\ \mathrm{W{\cdot}m^{-2}}$ remains to be studied at the cost of huge amounts of computing times. On the other hand, it has been conjectured above that at melting rates $Q > 15\,000\ \mathrm{W{\cdot}m^{-2}}$, melting will eventually develop from the outside of the ingot because, in practice, only the solidus point remains at a finite temperature. If this conjecture would be confirmed later, this should apply to the 1D system as well.

The errors in T_E, the transition temperature of the pure system, associated with the effect of two-front melting, are well within the standard uncertainty $u(T_\mathrm{E}) = 0.06\ \mathrm{K}$ attributed earlier to the eutectic Pt-C, disregarding the effect of two-front melting.

References

1. G. Machin, P. Bloembergen, J. Hartmann, M. Sadli, Y. Yamada, Int. J. Thermophys. **28**, 1976 (2007)
2. G. Machin, P. Bloembergen, K. Anhalt, J. Hartmann, M. Sadli, P. Saunders, E. Woolliams, Y. Yamada, H. Yoon, Int. J. Thermophys. **31**, 1779 (2010)
3. P. Bloembergen, H. Zhang, W. Dong, T. Wang, AIP Conf. Proc. **1552**, 340 (2013)
4. P. Bloembergen, W. Dong, C. Bai, T. Wang, Int. J. Thermophys. **32**, 2633 (2011)
5. W. Dong, T. Wang, P. Bloembergen, Y.Y. Duan, Int. J. Thermophys. **32**, 2680 (2011)
6. P. Castro, G. Machin, M.A. Villamañan, D. Lowe, Int. J. Thermophys. **32**, 1773 (2011)
7. G. Machin, P. Castro, A. Levick, M.A. Villamañan, Measurement **44**, 738 (2011)
8. V.R. Voller, A.D. Brent, C. Prakash, Int. J. Heat Mass Transfer **32**, 1719 (1989)
9. P. Castro, P. Bloembergen, A. Arroyo, Int. J. Thermophys. **35**, 438 (2014)
10. P. Bloembergen, Y. Yamada, N. Sasajima, Y. Wang, T. Wang, Metrologia **44**, 279 (2007)
11. D. Lowe, G. Machin, Metrologia **49**, 189 (2012)
12. P. Bloembergen, W. Dong, H. Zhang, T. Wang, Metrologia **50**, 295 (2013)

Table 1 Values for the main parameters used in the model for T_m

Function	T_{liq} (K)	T_E (K)	mc (K)	k	m (K)	c (mole fraction	c_{eut} (mole fraction)	T_{eut} (K)
T_m	2012.143	2012.229	-0.086	0.316	-915	9.4×10^{-5}	4.15×10^{-3}	2008.43

Table 2 Scheil function values for T_{cav} and $T_{backwall}$

Function	T_{liq} (K)	T_E (K)	mc (K)	k	m (K)	c (mole fraction)
T_{cav}	2012.019	2012.131	-0.113	0.415	-770	14.7×10^{-5}
$T_{backwall}$	2012.118	2012.229	-0.111	0.340	-1183	9.4×10^{-5}

Table 3 Thermophysical properties of the materials

Material	Thermal conductivity ($W \cdot m^{-1} \cdot K^{-1}$)	C_p ($J \cdot kg^{-1} \cdot K^{-1}$)	Density ($kg \cdot m^{-3}$)	Melting heat ($J \cdot kg^{-1}$)	Mass diffusivity ($m^2 \cdot s^{-1}$)
Pt-C	200 for T < 2011.957 K 100 for T > 2011.957 K	204.21	20214	134327.7	10^{-6}
Graphite	45.6	690	2250		
CC sheets	5	690	700		
Argon	1.6228	520.65	0.0158		

Table 4 Error ΔT_E in the eutectic temperature of the pure system, made when assuming inside melting only

Q ($W \cdot m^{-2}$)	F_{infl}	$F_{infl}^{(k-1)}$	ΔT_E (K)
3000	0.85	1.118	0.01
15 000	0.94	1.043	0.004

Figure Captions

Fig. 1 Cell scheme. Q in $W \cdot m^{-2}$. Scale: length of the ingot corresponds to 43 mm

Fig. 2 Freezing: impurity concentration $c(x, t)$ along x for different t; mass diffusivity = 10^{-6} $m^2 \cdot s^{-1}$

Fig. 3 Impurity concentration of the alloy after freeze. Impurity concentration, mole fraction, is defined on the color scale, given in the legend

Fig. 4 Liquid fraction distribution $F(x, t)$ during melting along x for different t and Q = 3000 $W \cdot m^{-2}$

Fig. 5 T_m, $T_{backwall}$, as modeled, and T_{cav}, as measured, as function of the liquid fraction $F = F(t)$ during melting. T_m: Q_f = -3000 $W \cdot m^{-2}$, T_{cav}: Q = 12 000 $W \cdot m^{-2}$, $T_{backwall}$: Q = 3000 $W \cdot m^{-2}$ and Q = 15 000 $W \cdot m^{-2}$

Fig. 6 Plateaus in terms of $T_{backwall}$ for freeze (Q_f = -3000 $W \cdot m^{-2}$) and melts for different Q (in $W \cdot m^{-2}$)

Fig. 7 Melting plateaus in terms of $T_{backwall}$ for different heat injection rates as function of the liquid fraction F

Fig. 8 Snapshots of the melting process for the impure systems Q = 3000 $W \cdot m^{-2}$ at (a) t = 4500 s, (b) t = 5100 s, and (c) t = 5250 s, and Q = 15 000 $W \cdot m^{-2}$ at (d) t = 3140 s, (e) t = 3270 s, and (f) t = 3280 s as well as for the pure system Q = 3000 $W \cdot m^{-2}$ at (g) t = 2310 s, (h) t = 2400 s, and (i) t = 2450 s. Liquid fractions are defined on the color scale, given in the legends, from close to zero (near to solid, in blue) to 1 (liquid state, in red).

Fig. 9 Melting plateaus in terms of $T_{backwall}$ for pure and impure systems as function of F for Q = 3000 $W \cdot m^{-2}$

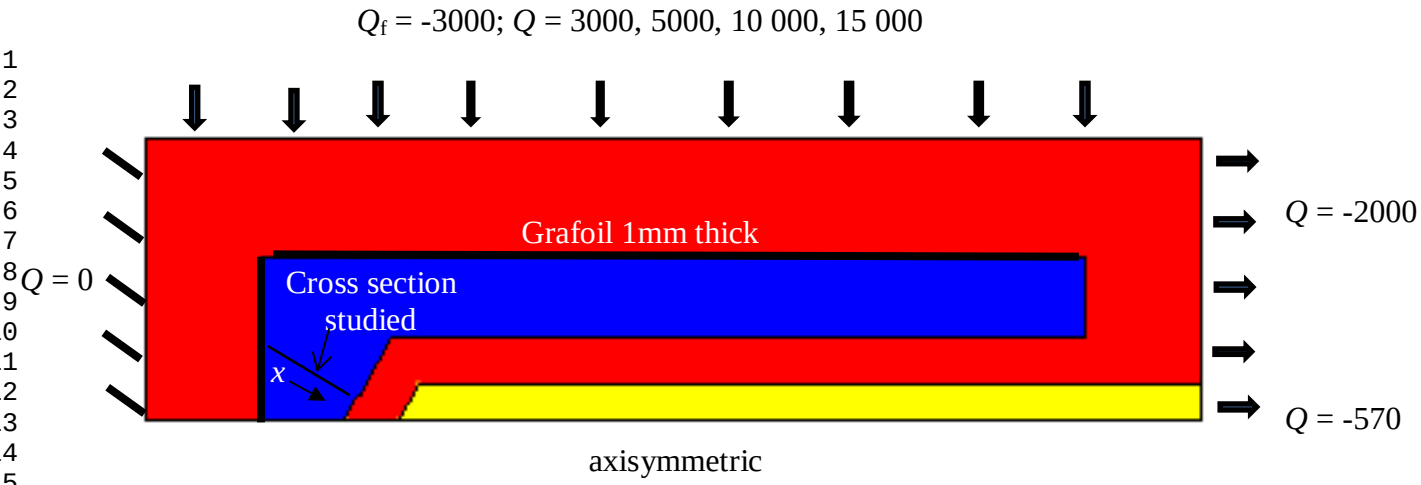
Q_f = -3000; Q = 3000, 5000, 10 000, 15 000
Grafoil 1mm thick
Cross section studied
x
Q = 0
Q = -2000
Q = -570
axisymmetric

Fig. 1

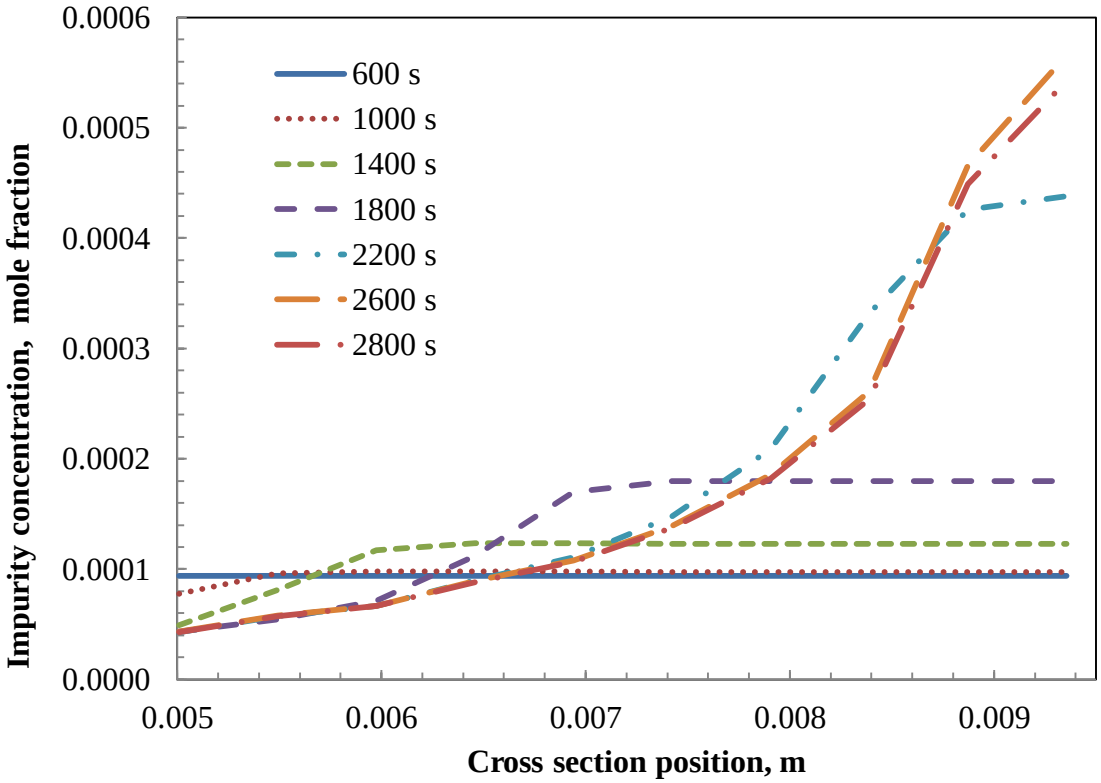
0.0006
0.0005
0.0004
0.0003
0.0002
0.0001
0.0000
Impurity concentration, mole fraction
600 s
1000 s
1400 s
1800 s
2200 s
2600 s
2800 s
0.005
0.006
0.007
0.008
0.009
Cross section position, m

Fig. 2

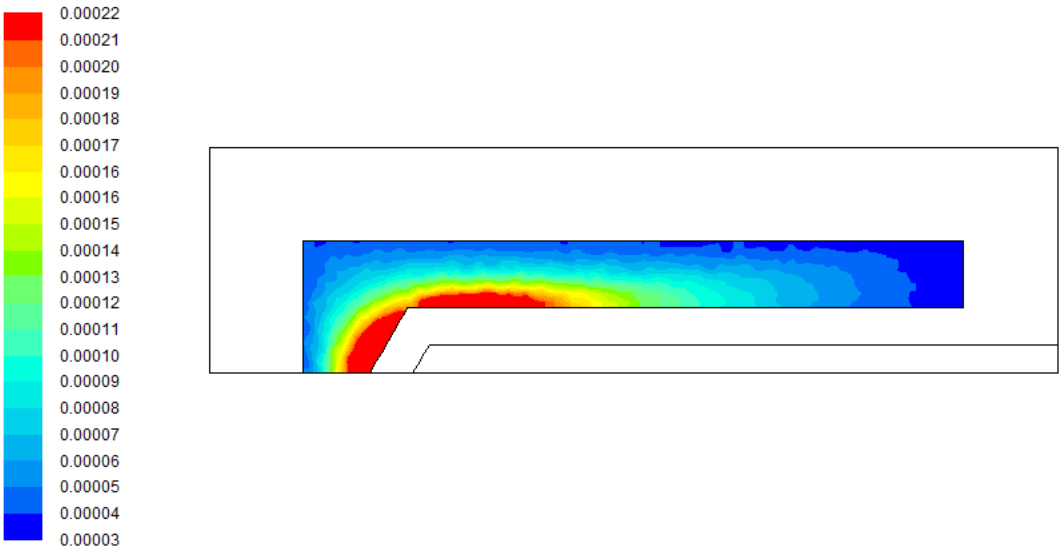
0.00022
0.00021
0.00020
0.00019
0.00018
0.00017
0.00016
0.00016
0.00015
0.00014
0.00013
0.00012
0.00011
0.00010
0.00009
0.00008
0.00007
0.00006
0.00005
0.00004
0.00003

Fig. 3

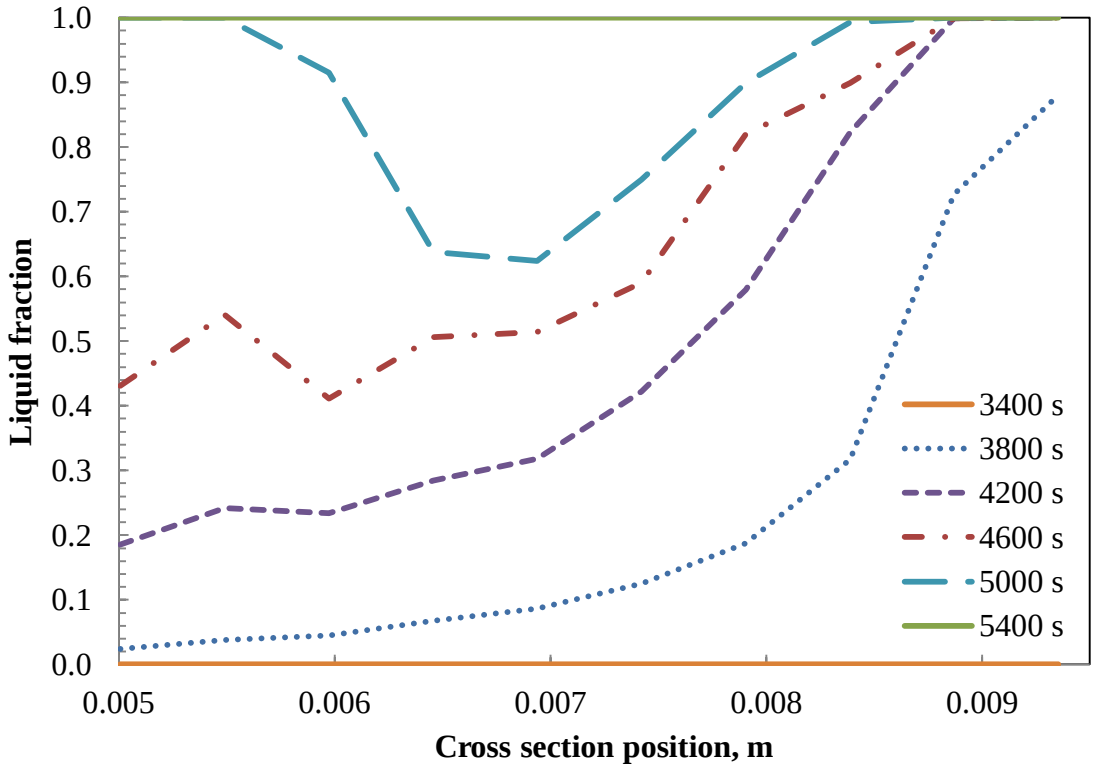
1.0
0.9
0.8
0.7
0.6
0.5
0.4
0.3
0.2
0.1
0.0
Liquid fraction
0.005
0.006
0.007
0.008
0.009
Cross section position, m
3400 s
3800 s
4200 s
4600 s
5000 s
5400 s

Fig. 4

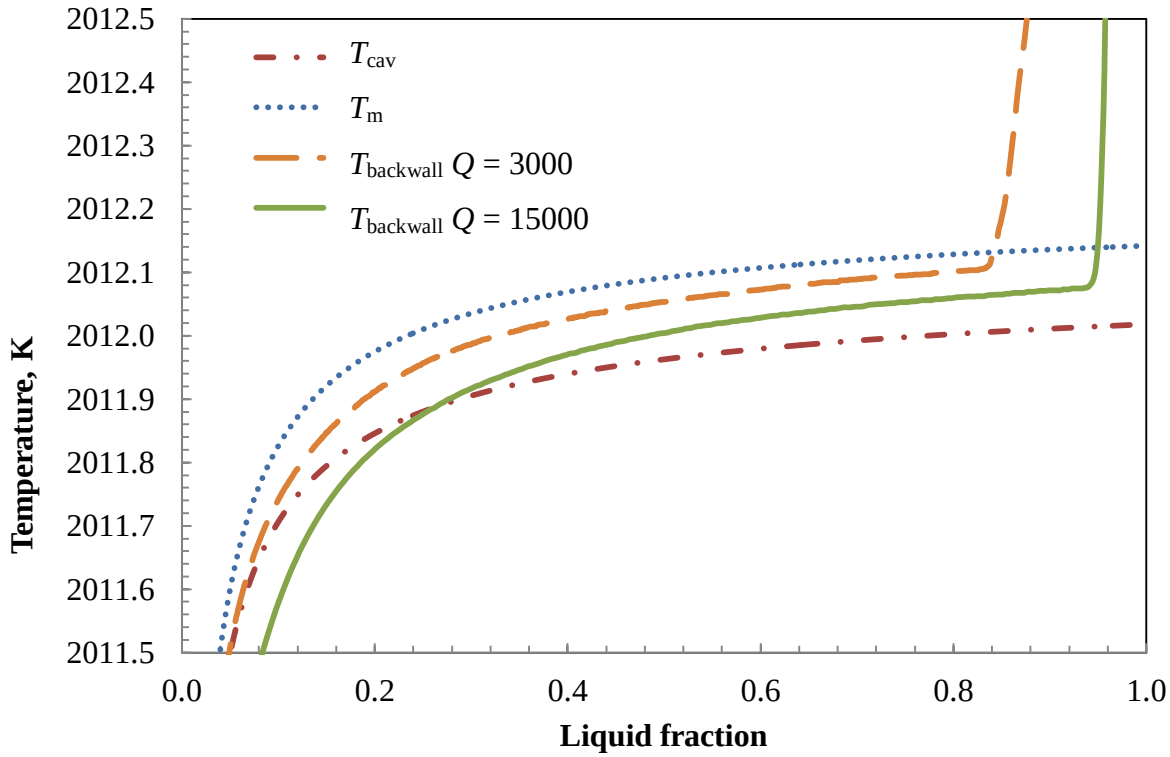
2012.5
2012.4
2012.3
2012.2
2012.1
2012.0
2011.9
2011.8
2011.7
2011.6
2011.5
Temperature, K
0.0
0.2
0.4
0.6
0.8
1.0
Liquid fraction
T_{cav}
T_m
$T_{backwall}$ Q = 3000
$T_{backwall}$ Q = 15000

Fig. 5

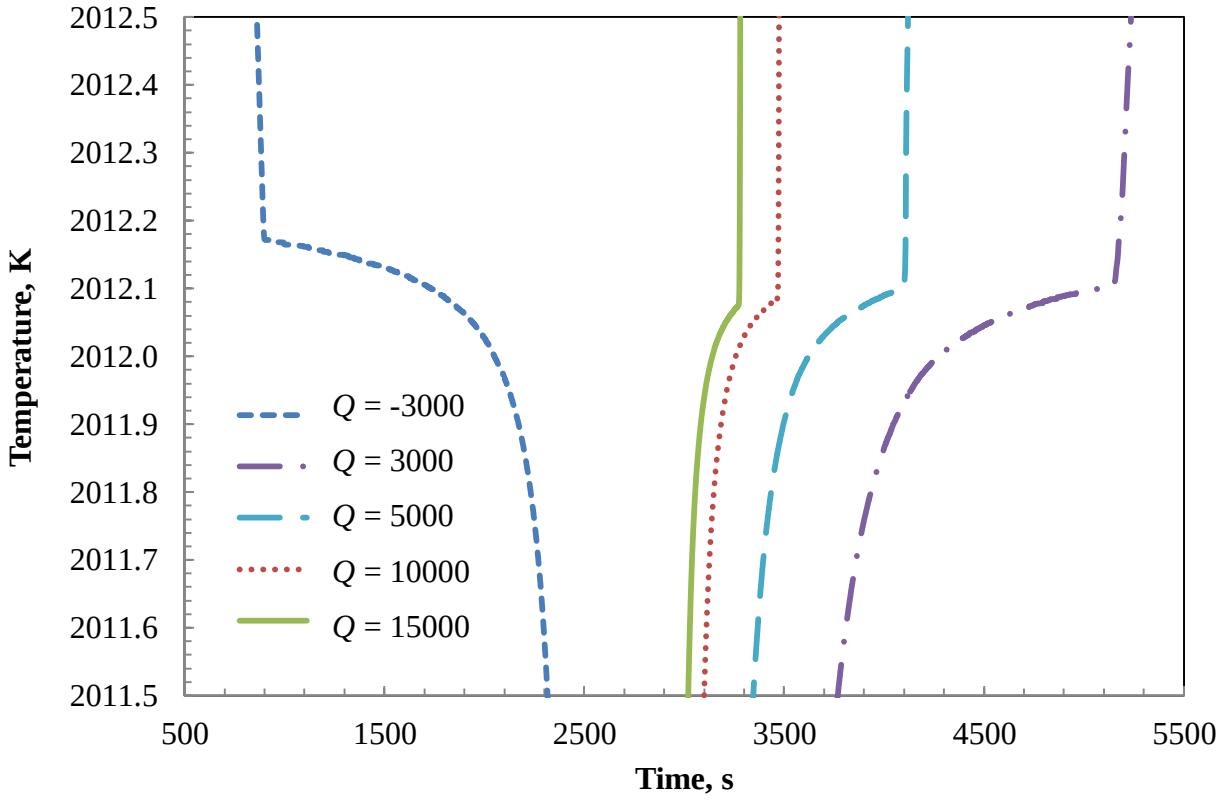
2012.5
2012.4
2012.3
2012.2
2012.1
2012.0
2011.9
2011.8
2011.7
2011.6
2011.5
Temperature, K
500
1500
2500
3500
4500
5500
Time, s
Q = -3000
Q = 3000
Q = 5000
Q = 10000
Q = 15000

Fig. 6

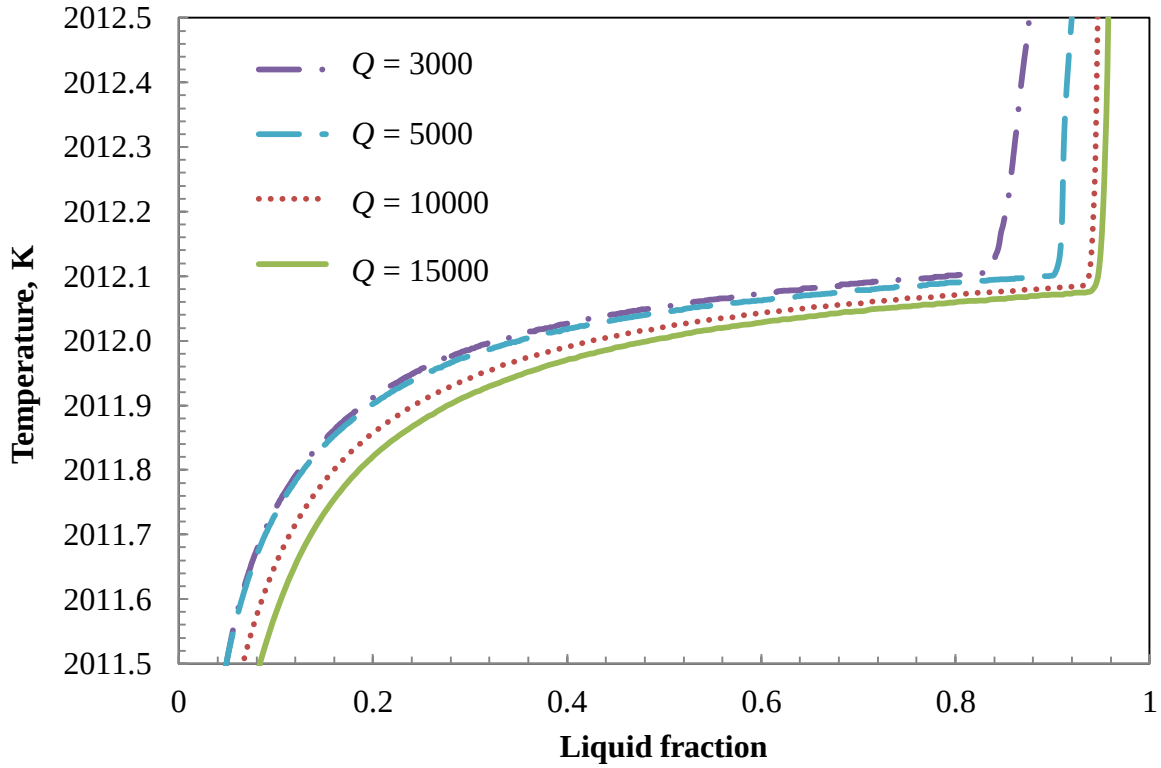
2012.5
2012.4
2012.3
2012.2
2012.1
2012.0
2011.9
2011.8
2011.7
2011.6
2011.5
Temperature, K
Q = 3000
Q = 5000
Q = 10000
Q = 15000
0
0.2
0.4
0.6
0.8
1
Liquid fraction

Fig. 7

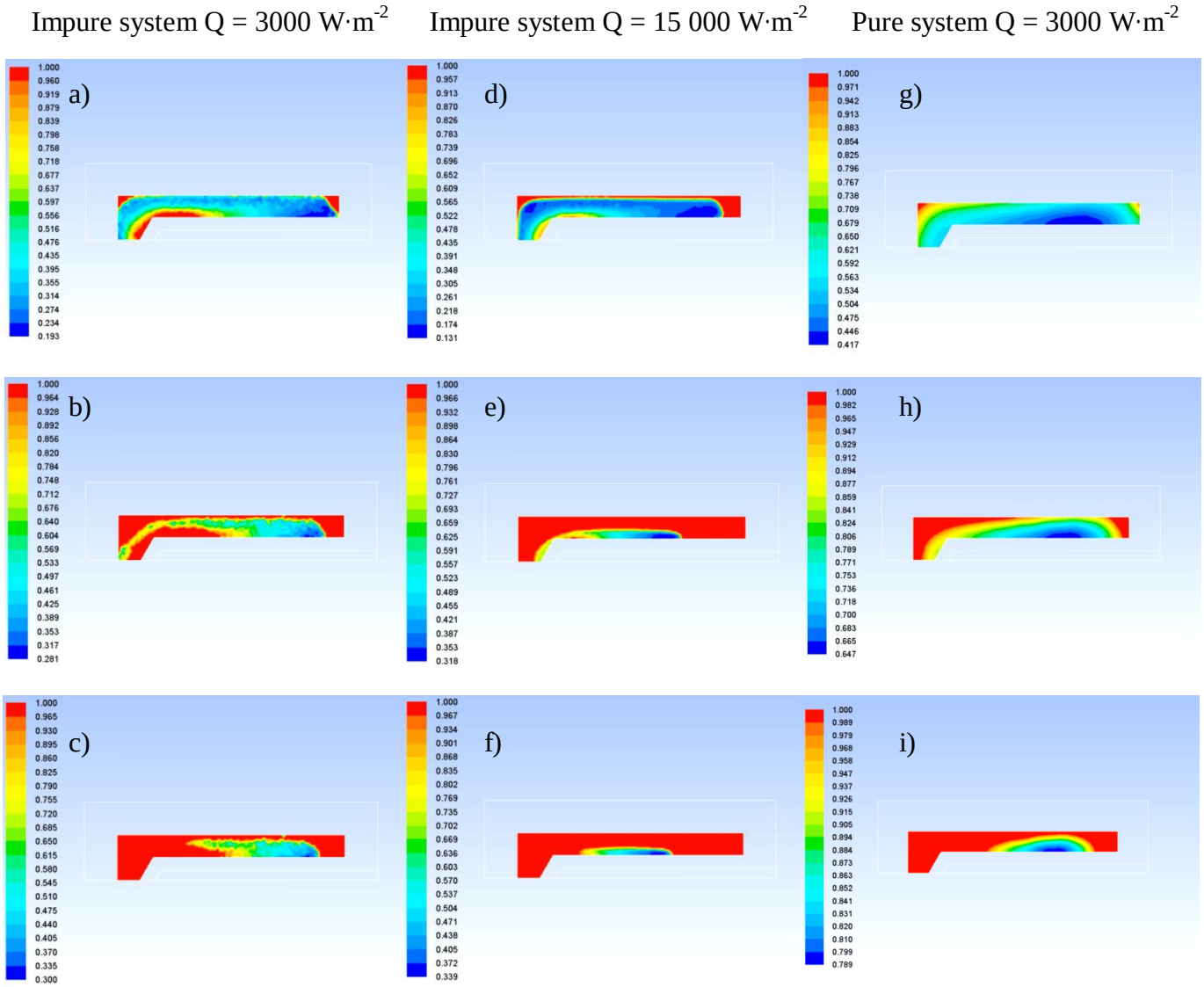
Impure system Q = 3000 W·m-2
Impure system Q = 15 000 W·m-2
Pure system Q = 3000 W·m-2
a)
b)
c)
d)
e)
f)
g)
h)
i)

Fig. 8

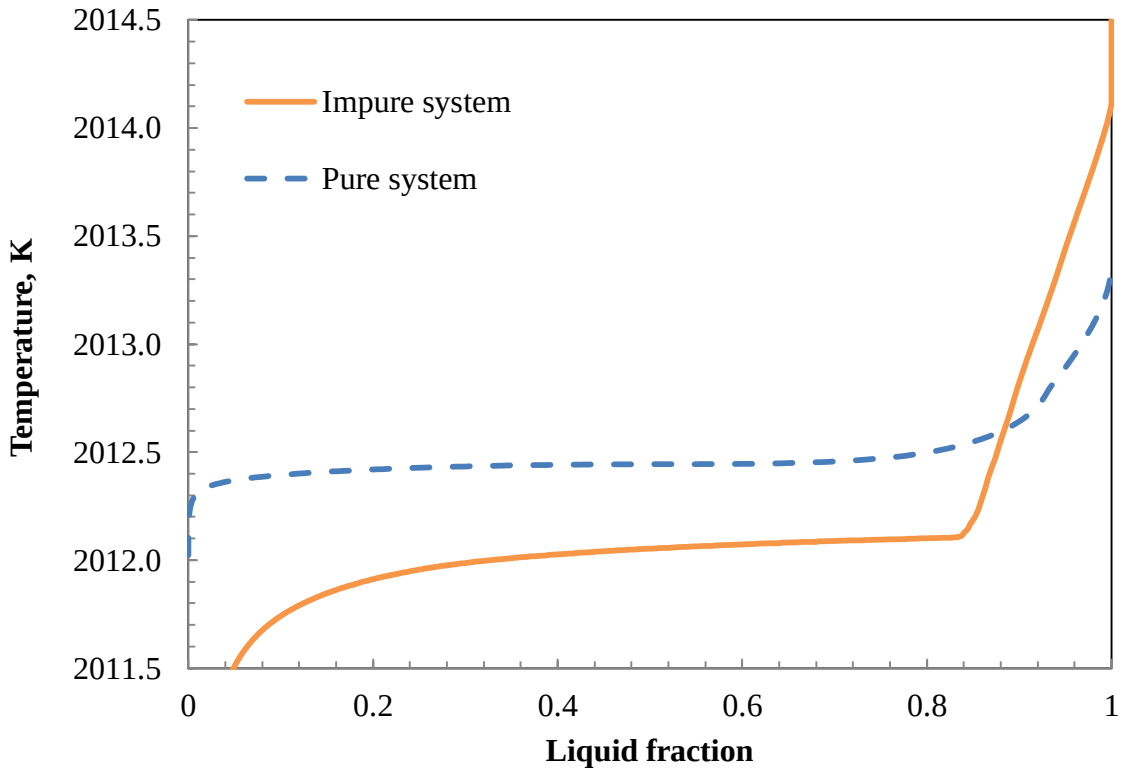
2014.5
2014.0
2013.5
2013.0
2012.5
2012.0
2011.5
Temperature, K
Impure system
Pure system
0
0.2
0.4
0.6
0.8
1
Liquid fraction

Fig. 9